Detection of periimplant fenestration and dehiscence with the use of two scan modes and the smallest voxel sizes of a cone-beam computed tomography device

Sergio Lins de-Azevedo-Vaz, DDS, MS,[a] Karla de Faria Vasconcelos, DDS, MS,[a]
Frederico Sampaio Neves, DDS, MS,[a] Saulo Leonardo Sousa Melo, DDS, MS,[a]
Paulo Sérgio Flores Campos, DDS, MS, PhD,[b] and Francisco Haiter-Neto, DDS, MS, PhD[a]
Piracicaba and Salvador, Brazil

Objective. To assess the accuracy of cone-beam computed tomography (CBCT) in periimplant fenestration and dehiscence detection, and to determine the effects of 2 voxel sizes and scan modes.
Study Design. One hundred titanium implants were placed in bovine ribs in which periimplant fenestration and dehiscence were simulated. CBCT images were acquired with the use of 3 protocols of the i-CAT NG unit: A) 0.2 mm voxel size half-scan (180°); B) 0.2 mm voxel size full-scan (360°); and C) 0.12 mm voxel size full scan (360°). Receiver operating characteristic curves and diagnostic values were obtained. The Az values were compared with the use of analysis of variance.
Results. The Az value for dehiscence in protocol A was significantly lower than those of B or C ($P < .01$). They did not statistically differ for fenestration ($P > .05$).
Conclusions. Protocol B yielded the highest values. The voxel sizes did not affect fenestration and dehiscence detection, and for dehiscence full-scan performed better than half-scan. (Oral Surg Oral Med Oral Pathol Oral Radiol 2013;115:121-127)

In the literature it has been seen that it is necessary to have at least 1 mm of bone around the implant if the treatment is to be successful.[1] However, unfavorable anatomic conditions can cause insufficient bone volume and result in incorrect positioning of the implant, which leads to the occurrence of complications such as cortical bone defects, including fenestrations and dehiscences. Periimplant dehiscence is characterized by the absence of bone initiating from the cervical portion of the implant. The absence of bone in part of the implant, with bone at the coronal portion, is called periimplant fenestration. Dehiscence and fenestration may be caused by incorrect placement of the implant during surgery, and, in addition, there could be 2 other etiologic factors involved: excessive loading, and inflammation caused by biofilm. These defects prevent the implant surface from being completely covered, thereby compromising esthetics and hygiene.[1] An early diagnosis of periimplant bone defects is of paramount importance, because such defects can lead to gingival recession and bone and implant loss.[2]

Currently, the intraoral periapical radiograph using the long-cone paralleling technique is the standard method for the longitudinal assessment of dental implants. This technique uses low radiation doses and involves lower costs. It can be done chairside[3] and provides sufficient accuracy for postoperative implant assessment.[4-6] However, the periapical radiograph is limited in that it only provides 2-dimensional images, which are unhelpful when determining whether or not periimplant fenestration or dehiscence is present, because only interproximal bone assessment is possible.[7] Cone-beam computed tomography (CBCT) provides 3-dimensional images of the cortical bone adjacent to the dental implant, which allows for complete visualization of the vestibular and lingual cortical plates. Therefore, reentry procedures to assess bone around dental implants, as in periimplant fenestration and dehiscence cases, could be avoided by using CBCT examinations.[3]

The literature has stated that the postoperative assessment of dental implants with the use of CBCT is compromised by the artefacts induced by titanium, i.e., beam-

Statement of Clinical Relevance

This paper presents relevant data regarding the impairment caused by the artefacts induced by titanium in the diagnosis of periimplant cortical defects. This difficulty has not been previously measured, and CBCT parameters have not been previously tested to minimize these artefacts.

Neodent supplied the implants used in this research.
[a]Department of Oral Diagnosis, Division of Oral Radiology, Piracicaba Dental School, State University of Campinas, Piracicaba, São Paulo, Brazil.
[b]Department of Oral Radiology, Division of Oral Radiology, School of Dentistry, Federal University of Bahia, Salvador, Bahia, Brazil.
Received for publication Jun 7, 2012; return for revision Oct 9, 2012; accepted for publication Oct 15, 2012.

2212-4403/$ - see front matter
http://dx.doi.org/10.1016/j.oooo.2012.10.003

hardening artefacts.[7] It is known that voxel size and scan mode (180°/360°) can both benefit CBCT image quality and improve the diagnosis of certain conditions.[8-13] However, the effect of these exposure parameters in beam-hardening artefact reduction and in the detection of periimplant cortical defects has not been studied. The accuracy of CBCT in diagnosing periimplant fenestration and dehiscence also has not been determined, even though it had been for the dental counterparts.[2,14]

Against this background, the present study set out to assess the accuracy of CBCT in the diagnosis of periimplant fenestration and dehiscence and to determine the effects of 2 small voxel sizes and 2 scan modes of a CBCT unit. The variables in the study were the presence/absence of fenestration and dehiscence, and the factors in the study were voxel size and scan mode.

MATERIALS AND METHODS

This study design received full approval from the local Research Ethics Committee at the Piracicaba Dental School, State University of Campinas (protocol 084/2011). With a standard preparation machine[15] and a spherical bur (3017HL; KG Sorensen, São Paulo, SP, Brazil), an operator performed defects to simulate fenestration and dehiscence in fragments of fresh bovine ribs. These defects were 2.5 mm in diameter, with an elliptic form for fenestration and a half-elliptic form for dehiscence. Bovine ribs were used to simulate the alveolar bone tomographic aspect.[16]

The dehiscence defects were created on an edge of the bovine rib, which would correspond to the cervical portion of the implant to be placed. The fenestration defects were performed at 10 mm from the rib edge, to correspond to the apical portion of the implant. The defects were randomly distributed over the cervical and/or apical sites. After all the defects had been created, an oral surgeon with experience in implant dentistry placed 100 3.75 × 11 mm titanium implants (Titamax; Neodent, Curitiba, PR, Brazil) in the ribs.

The ribs with the implants were then placed in a container with water to simulate soft tissue attenuation, and CBCT acquisition was performed with the i-CAT Next Generation (NG) unit (Imaging Sciences International, Hatfield, PA) with a field of view (FOV) size of 8 × 8 cm. Three protocols were used: 0.2 mm voxel size half-scan (180°) (protocol A), 0.2 mm voxel size full-scan (360°) (protocol B), and 0.12 mm voxel size full scan (360°) (protocol C). Their specifications and exposure parameters are described in Table I. The final sample comprised 100 sites for evaluation of fenestration (50 with defects and 50 without) and 100 sites for the evaluation of dehiscence (50 with defects and 50 without). Figure 1 illustrates examples of implants with and without defects.

Table I. Exposure parameters of the protocols tested

Protocol	*Voxel*	*Scan*	*Exposure time*	*mAs*
A	0.2 mm	180°	14.7 s	20.27
B	0.2 mm	360°	26.9 s	37.07
C	0.12 mm	360°	26.9 s	37.07

The kilovoltage and miliamperage parameters were set at 120 and 5, respectively

Three oral radiologists with at least 3 years' experience in CBCT were previously calibrated for the experiment. They blindly evaluated all the images in Xorancat software version 3.0.34 (Xoran Technologies, Ann Arbor, MI), under dim lighting conditions. They could adjust brightness and contrast and use the zoom tool, but task-specific filters were not permitted. The evaluation adopted a 5-point scale for presence/absence of defects (1, definitely absent; 2, probably absent; 3, uncertain; 4, probably present; 5, definitely present). The images were reevaluated after 30 days. Inter- and intraobserver agreements were calculated with the use of the kappa test (poor agreement, 0.40; moderate agreement, 0.40-0.59; good agreement, 0.60-0.74; excellent agreement, 0.75-1.00).

The responses were tabulated with the criterion standard (obtained through a macroscopic analysis of the bovine ribs) and plotted into a web-based calculator for receiver operating characteristic (ROC) curves (Russell H. Morgan Department of Radiology and Radiological Science, Johns Hopkins University, Baltimore, MD).[17] The ROC analysis was performed by pooling observer responses, and the diagnostic values of the protocols tested were calculated. The areas under the ROC curves (Az values) in the protocols were compared with the use of 1-way analysis of variance (ANOVA) with the Bonferroni post hoc test, adopting a 5% significance level. The null hypothesis assumed no statistical difference between scan modes (protocols A and B) or between voxel sizes (protocols B and C). Reliability statistics and ANOVA were performed in the SPSS software package version 17.0 for Windows (SPSS, Chicago, IL).

RESULTS

Reliability statistics for intra- and interobserver agreement resulted in excellent kappa values for fenestration, and the values for dehiscence ranged from moderate to excellent agreement (Table II).

The Az values for the observers are summarized in Table III. There was no statistically significant difference between the protocols tested for fenestration. For dehiscence, however, protocol A had lower Az values that were statistically different from protocols B and C.

Table IV presents the sensitivity, specificity, accuracy, positive predictive value (PPV), and negative predictive value (NPV) for the protocols. For both

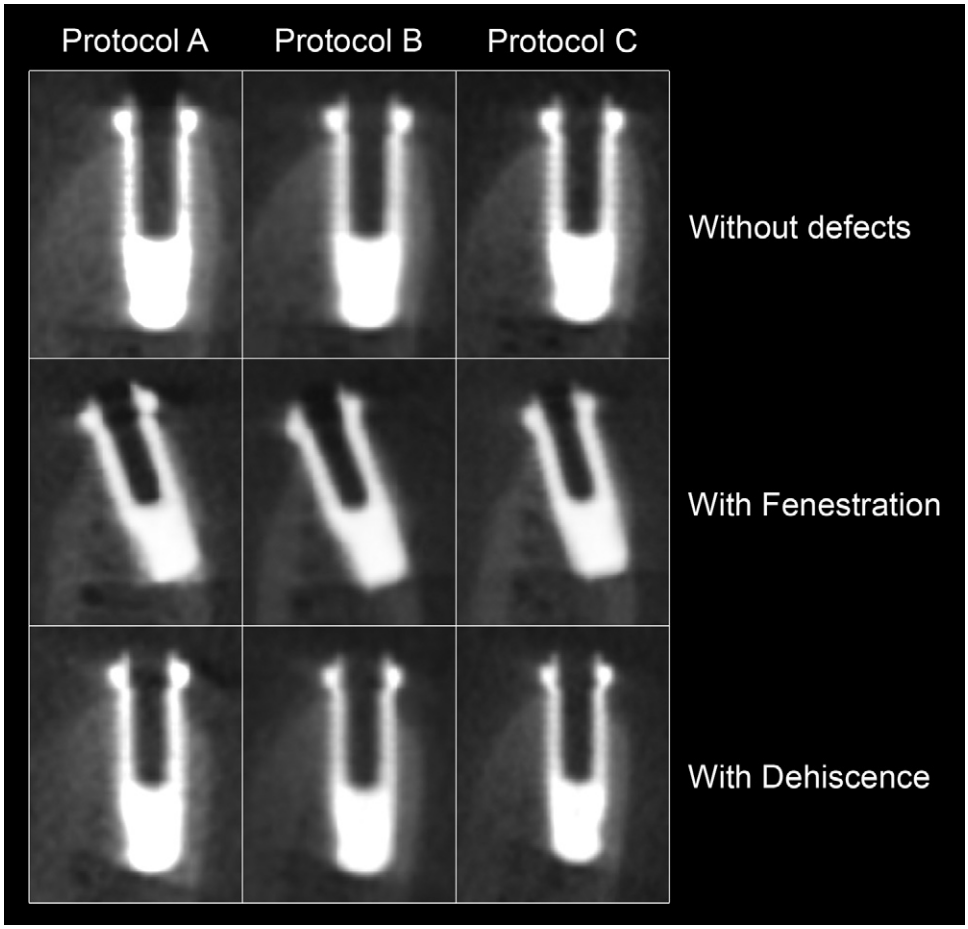

Fig. 1. CBCT sagittal slices showing implants with and without defects. Protocol A: 0.2 mm voxel size, half-scan (180°); protocol B: 0.2 mm voxel size, full-scan (360°); protocol C: 0.12 mm voxel size, full-scan (360°).

Table II. Kappa values for intra- and interobserver agreements

	Protocol A			*Protocol B*			*Protocol C*		
	Obs. 1	*Obs. 2*	*Obs. 3*	*Obs. 1*	*Obs. 2*	*Obs. 3*	*Obs. 1*	*Obs. 2*	*Obs. 3*
Fenestration									
Obs. 1	0.89	—	—	0.89	—	—	0.80	—	—
Obs. 2	0.87	0.76	0.81	0.82	0.79	0.80	0.80	0.77	0.79
Obs. 3	0.79	—	1.00	1.00	—	1.00	0.80	—	1.00
Dehiscence									
Obs. 1	0.42	—	—	0.61	—	—	0.64	—	—
Obs. 2	0.44	0.41	0.41	0.66	0.60	0.76	0.65	0.61	0.67
Obs. 3	0.48	—	0.40	0.66	—	0.62	0.61	—	0.63

Protocol A: 0.2 mm voxel size, half-scan (180°); protocol B: 0.2 mm voxel size, full-scan (360°); protocol C: 0.12 mm voxel size, full-scan (360°).
Obs., Observer.

fenestration and dehiscence, these values were highest in protocol B and lowest in protocol A.

DISCUSSION

Periapical radiographs are usually used in the postoperative evaluation of dental implants, because they are more accurate than CBCT in determining if osseointegration has occurred or there is periimplantitis.[18] They are also used in assessing the interproximal periimplant bone level.[3] A recent study has also shown that digital periapical radiography may provide a faster and more confident diagnosis, with accuracy similar to film-based periapical radiography.[19] However, when conventional radiographs are incapable of offering sufficient information, e.g., when periimplant fenestration and/or dehiscence are suspected, CBCT should be considered as

Table III. Area under the receiver operating characteristic curve (Az values) for the observers in the protocols tested

	Obs. 1	*Obs. 2*	*Obs. 3*	*Mean (SD)*
Fenestration				
Protocol A	0.87	0.89	0.92	0.89 (0.03)*
Protocol B	0.95	0.89	0.95	0.93 (0.03)*
Protocol C	0.92	0.94	0.97	0.94 (0.03)*
Dehiscence				
Protocol A	0.68	0.69	0.66	0.68 (0.02)†
Protocol B	0.76	0.72	0.74	0.74 (0.02)‡
Protocol C	0.75	0.73	0.71	0.73 (0.02)‡

Abbreviations as in Table II.
*Difference not significant ($P > .05$).
†Statistically different from ($P < .01$).
‡Statistically different from ($P < .01$).

Table IV. Diagnostic values for the protocols tested

	Sensitivity	*Specificity*	*Accuracy*	*PPV*	*NPV*
Fenestration					
Protocol A	0.87	0.85	0.86	0.84	0.86
Protocol B	0.90	0.95	0.93	0.95	0.90
Protocol C	0.89	0.94	0.92	0.93	0.89
Dehiscence					
Protocol A	0.53	0.69	0.61	0.63	0.59
Protocol B	0.56	0.75	0.66	0.70	0.63
Protocol C	0.55	0.75	0.65	0.69	0.63

PPV, Positive predictive value; *NPV*, negative predictive value; other abbreviations as in Table II.

a means of avoiding reentry procedures.[3] It has already been shown that CBCT can precisely determine cortical bone thickness adjacent to dental implants, especially when a smaller voxel size is used.[16] It is also accurate in measuring periodontal and periimplant defects, and provides higher image quality than computed tomography or periapical or panoramic radiographs.[2,20]

The literature has discussed how beam-hardening artefacts could obscure the diagnosis of periimplant defects and the visualization of the bone-implant surface.[7,21] The beam-hardening artefact occurs particularly in the presence of high-density materials (e.g., amalgam crowns), but also to a lesser extent with light metals, such as titanium.[22] The implant acts as a filter, making the polychromatic X-ray beam become "harder," i.e., with wavelengths of higher energy.[21,22] Therefore, the gray values of an image are lower than they would be without the titanium. The effect of beam-hardening in our experiment can be seen in Figure 2. In the implant without defects, the beam-hardening artefact is considerably noticeable (*white arrows*), simulating fenestration and dehiscence defects. Therefore, the evaluation of the periimplant cortical plates must be undertaken with great care to avoid false-positive conclusions.

In some situations, bone volume is limited and analysis of the cortical plate adjacent to a dental implant is difficult. Figure 2 also illustrates a situation in which thin cortical bone can be deemed to be unreadable (*black arrows*). However, studies have shown that it may be possible to postoperatively evaluate dental implants even in thinner cortical plates.[2,16,23,24] The results of our study corroborate those papers, because the diagnostic values found for both fenestrations and dehiscences were considered to be clinically acceptable. This conclusion can be drawn when the sum of either sensitivity plus specificity or PPV plus NPV are considered. According to Blicher et al. (2005),[25] a measure presents good validity when this value is 1.20 or above. In the present study, the lowest sum of sensitivity plus specificity and PPV plus NPV was found in protocol A for dehiscence (1.22).

In addition, our results showed that it was easier to detect fenestration than dehiscence. The kappa values showed excellent interobserver agreement for fenestration whereas for dehiscence they ranged from moderate to excellent. Intraobserver agreement for dehiscence was also lower than for fenestration, and this demonstrated how difficult and uncertain it is even for the same observer to determine whether or not periimplant dehiscence is present. Diagnosing periimplant fenestration can be particularly easy if the implant is considerably angulated (Figure 1). On the other hand, the closeness of the marginal bone and soft tissue density values makes the detection of dehiscence in CBCT a difficult task. When the defect occurs adjacent to a dental implant, the dark areas produced by the beam-hardening artefact makes it even more difficult. This is clearly demonstrated through the lower sensitivity and NPV values attributed for dehiscence, which indicated a high false-negative rate. Similarly, a study by Raes et al. (2011)[3] had shown that CBCT significantly underrated the interproximal periimplant bone level. We simulated 2.5 mm dehiscence defects, i.e., initial bone loss. Studies evaluating larger defects are recommended to determine if those can be diagnosed more easily.

Voxel size is directly linked to the spatial resolution of an image. In general, the smaller the voxel size, the better both resolution and details.[26] So this study applied the smallest voxel sizes of the i-CAT NG unit to assess the accuracy of CBCT in the detection of periimplant dehiscence and fenestration, by using the best resolution and details possible. On analyzing the Az values, it can be seen that the 0.12 mm voxel size (protocol C) was not statistically different from the 0.2 mm (protocol B) for both defects. Thus, the voxel sizes tested did not influence accuracy in fenestration or dehiscence detection. In fact, the 0.12 mm voxel size had slightly lower diagnostic values than the 0.2 mm

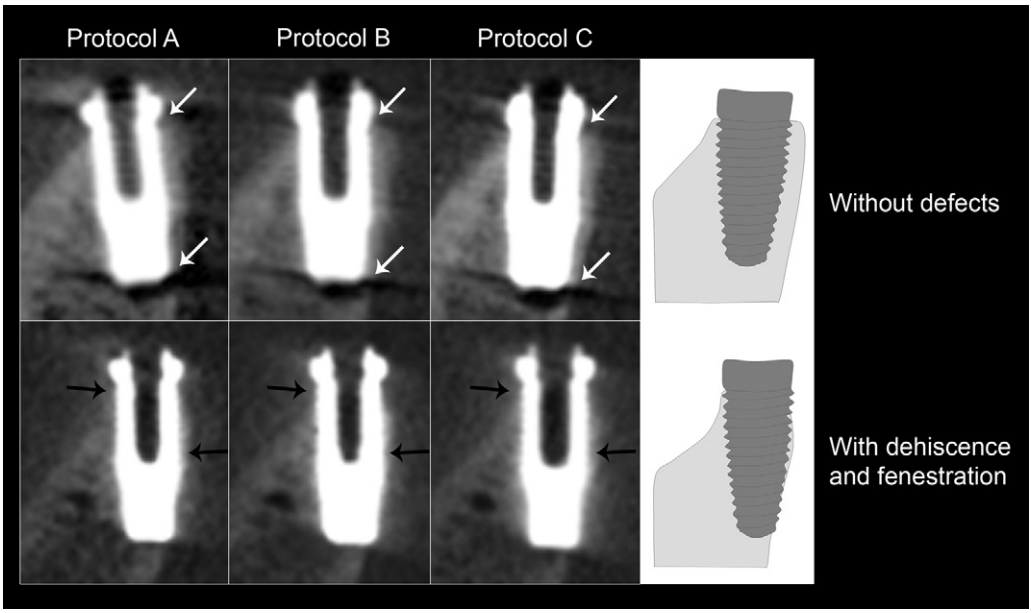

Fig. 2. The symmetric disposition of the hypodense lines in both sides of the implant (*white arrows*) is strong evidence of beam-hardening artefact. The *black arrows* indicate thin cortical bone which is hardly seen in the slices.

voxel size. We think that the difference in size of the voxels tested might not have been sufficient to increase the spatial resolution of the images to any significant degree. Furthermore, other studies have shown that voxel size exerts little influence on the detection of external root resorption,[8,27] internal root resorption,[9] occlusal caries,[28] root fractures,[10,29] or preoperative implant measurements.[13,30]

Larger voxel sizes (e.g., 0.3 and 0.4 mm) would probably result in lower Az values. However, they were not included in the present investigation because Razavi et al. (2010)[16] had already shown that a 0.3 mm voxel size produced insufficient resolution of the cortical bone adjacent to dental implants. Clinical studies also use small voxel sizes for postoperative implant assessment, because thin cortical bone can be deemed to be unreadable by CBCT.[3,24]

The signal of an image is compiled from the multiangular images (frames) produced during the image acquisition cycle. It is known that an increase in the angular images acquired will increase the signal.[26] However, a reliable representation of the object scanned can be obtained from a finite number of projections from at least 180° around the object.[21] Therefore, the present study also tested to see if the half-scan mode would be different from that of the full-scan mode for fenestration and dehiscence detection. The results indicated that the half-scan mode (protocol A) was similar to the full-scan mode (protocol B) for fenestration, whereas for dehiscence it was statistically worse. However, other studies have reported better results for the half-scan mode in implant planning[31] and in the detection of periapical lesion[11] and external root resorption.[12] Those studies also considered the relationship between the dose applied in the half-scan mode and its accuracy. It is known that exposure time directly influences the radiation dose of CBCT examinations. The half-scan mode is linked to lower X-ray radiation doses, because the exposure time used is lower than for the full-scan mode. We did not compare half-scan with full-scan using 0.12 mm voxel size, because the i-CAT NG unit allows only full-scan for this voxel size.

To the best of our knowledge, few studies have been done to assess the effective doses for the i-CAT NG with an FOV of 8 × 8 cm. A recent publication by Morant et al. (2012)[32] found that the organ doses for half-scan were ~40% lower than those calculated for full-scan. Those authors applied an FOV of 8 × 8 cm, but with standard resolution (0.3 and 0.4 mm voxel sizes), which requires lower exposure time. A study by Grunheid et al. (2012)[33] indicated an effective dose of 134.2 μSv (approximately the dose of 6 panoramic radiographs) for the 0.2 mm, 8 × 8 cm, full-scan protocol. Ludlow and Ivanovic (2008)[34] found higher effective doses with the use of full-scan in the Prexion 3D (189 μSv) and CB Mercuray (407 μSv) units.

The International Commission on Radiological Protection (2007)[35] and the Safety and Efficacy of a New and Emerging Dental X-ray Modality project (2012)[36] state that high-quality images are not essential for all diagnostic tasks, and the quality level depends on the diagnostic task. Excessive dose reduction may ad-

versely affect image quality and decrease lesion detection. Accordingly, considering both defects, we recommend that full-scan CBCT be used, because a smaller FOV (including only the region of interest) can be selected. Routine postoperative CBCT examinations for detection of periimplant fenestration or dehiscence are discouraged, because the acquisition should be indicated only if such defects are suspected and when a patient would benefit from their detection.

In clinical practice, the detection of fenestration and dehiscence in CBCT may have lower accuracy, owing to the presence of teeth, metallic dental fillings, or other producers of artefacts. Bovine ribs do not directly reflect the clinical situation, where there are more structures in the path of the X-ray beam. However, this experimental model provides a valuable estimation of what happens in vivo. One example is that in our experience, we have noticed that it is easier to determine the presence of a fenestration defect than dehiscence. This is also valid when these defects occur near teeth. Leung et al. (2010)[14] observed similar sensitivity and specificity values to those of our study, despite the fact that higher NPVs (≥0.95) and lower PPVs (dehiscence 0.50, fenestration 0.25) were found. These differences are probably due to different methodology and fewer artefacts, because those authors studied dental fenestrations and dehiscences.

The results presented in the present study refer only to the i-CAT NG device, because other equipment may provide different results given the specifications of the image receptor (flat-panel, image intensifier, or CMOS), the X-ray source (kilovoltage and miliamperage), method of X-ray generation (pulsed or continuous), voxel size, and FOV used. These parameters produce different image quality and noise, depending on the CBCT machine considered.[37]

CONCLUSION

Protocol B yielded the highest diagnostic values for periimplant fenestration and dehiscence both. The former can be detected very well in half-scan (180°) CBCT examinations, whereas diagnosing periimplant dehiscence requires full-scan (360°). The 0.12 mm voxel size was not any better than the 0.2 mm voxel size for both periimplant cortical defects. The full-scan mode, however, seems to minimize the artefacts, given the better results for dehiscence. Quantitative studies analyzing these parameters in beam-hardening reduction are encouraged to clarify these issues. Based on our findings, we recommend that preference be given to full-scan CBCT with 0.2 mm voxel size, using a small FOV, to evaluate the integrity of the periimplant cortical plates.

REFERENCES

1. Blanco J, Alonso A, Sanz M. Long-term results and survival rate of implants treated with guided bone regeneration: a 5-year case series prospective study. Clin Oral Implants Res 2005; 16:294-301.
2. Mengel R, Kruse B, Flores-de-Jacoby L. Digital volume tomography in the diagnosis of peri-implant defects: an in vitro study on native pig mandibles. J Periodontol 2006;77:1234-41.
3. Raes F, Renckens L, Aps J, Cosyn J, Bruyn H. Reliability of circumferential bone level assessment around single implants in healed ridges and extraction sockets using cone beam CT. Clin Implant Dent Relat Res 2011. [In press].
4. de Smet E, Jacobs R, Gijbels F, Naert I. The accuracy and reliability of radiographic methods for the assessment of marginal bone level around oral implants. Dentomaxillofac Radiol 2002;31:176-81.
5. Wakoh M, Harada T, Otonari T, Otonari-Yamamoto M, Ohkubo M, Kousuge Y, et al. Reliability of linear distance measurement for dental implant length with standardized periapical radiographs. Bull Tokyo Dent Coll 2006;47:105-15.
6. Adriaens PA, de Boever J, vande Velde F. Comparison of intraoral long-cone paralleling radiographic surveys and orthopantomographs with special reference to the bone height. J Oral Rehabil 1982;9:355-65.
7. Angelopoulos C, Aghaloo T. Imaging technology in implant diagnosis. Dent Clin North Am 2011;55:141-58.
8. Liedke GS, da Silveira HE, Silveira HL, Dutra V, de Figueiredo JA. Influence of voxel size in the diagnostic ability of cone beam tomography to evaluate simulated external root resorption. J Endod 2009;35:233-5.
9. Kamburoğlu K, Kursun S. A comparison of the diagnostic accuracy of CBCT images of different voxel resolutions used to detect simulated small internal resorption cavities. Int Endod J 2010;43:798-807.
10. Melo SL, Bortoluzzi EA, Abreu M Jr, Corrêa LR, Corrêa M. Diagnostic ability of a cone-beam computed tomography scan to assess longitudinal root fractures in prosthetically treated teeth. J Endod 2010;36:1879-82.
11. Lennon S, Patel S, Foschi F, Wilson R, Davies J, Mannocci F. Diagnostic accuracy of limited-volume cone-beam computed tomography in the detection of periapical bone loss: 360° scans versus 180° scans. Int Endod J 2011;44:1118-27.
12. Durack C, Patel S, Davies J, Wilson R, Mannocci F. Diagnostic accuracy of small volume cone beam computed tomography and intraoral periapical radiography for the detection of simulated external inflammatory root resorption. Int Endod J 2011; 44:136-47.
13. Waltrick KB, de Abreu Junior MJ, Corrêa M, Zastrow MD, d'Avila Dutra V. Accuracy of linear measurements and visibility of the mandibular canal on cone-beam computed tomography images with different voxel sizes: an in vitro study. J Periodontol. [In press].
14. Leung CC, Palomo L, Griffith R, Hans MG. Accuracy and reliability of cone-beam computed tomography for measuring alveolar bone height and detecting bony dehiscences and fenestrations. Am J Orthod Dentofacial Orthop 2010;137:S109-19.
15. Soares CJ, Fonseca RB, Gomide HA, Correr-Sobrinho L. Cavity preparation machine for the standardization of in vitro preparations. Braz Oral Res 2008;22:281-7.
16. Razavi T, Palmer RM, Davies J, Wilson R, Palmer PJ. Accuracy of measuring the cortical bone thickness adjacent to dental implants using cone beam computed tomography. Clin Oral Implants Res 2010;21:718-25.

17. Eng J. ROC analysis: web-based calculator for ROC curves; updated 2006. Baltimore (MD): Johns Hopkins University. Available at: http://www.jrocfit.org/.
18. Dave M, Davies J, Wilson R, Palmer R. A comparison of cone beam computed tomography and conventional periapical radiography at detecting peri-implant bone defects. Clin Oral Implants Res. [In press].
19. Sirin Y, Horasan S, Yaman D, Basegmez C, Tanyel C, Aral A, Guven K. Detection of crestal radiolucencies around dental implants: an in vitro experimental study. J Oral Maxillofac Surg 2012;70:1540-50.
20. Mengel R, Candir M, Shiratori K, Flores-de-Jacoby L. Digital volume tomography in the diagnosis of periodontal defects: an in vitro study on native pig and human mandibles. J Periodontol 2005;76:665-73.
21. Schulze RK, Berndt D, d'Hoedt B. On cone-beam computed tomography artifacts induced by titanium implants. Clin Oral Implants Res 2010;21:100-7.
22. Schulze R, Heil U, Gross D, Bruellmann DD, Dranischnikow E, Schwanecke U, Schoemer E. Artefacts in CBCT: a review. Dentomaxillofac Radiol 2011;40:265-73.
23. Shiratori LN, Marotti J, Yamanouchi J, Chilvarquer I, Contin I, Tortamano-Neto P. Measurement of buccal bone volume of dental implants by means of cone-beam computed tomography. Clin Oral Implants Res 2012;23:797-804.
24. Naitoh M, Nabeshima H, Hayashi H, Nakayama T, Kurita K, Ariji E. Postoperative assessment of incisor dental implants using cone-beam computed tomography. J Oral Implantol 2010;36:377-84.
25. Blicher B, Joshipura K, Eke P. Validation of self-reported periodontal disease: a systematic review. J Dent Res 2005;84:881-90.
26. Hatcher DC. Operational principles for cone-beam computed tomography. J Am Dent Assoc 2010;3:3S-6S.
27. Neves FS, Vasconcelos TV, Vaz SL, Freitas DQ, Haiter-Neto F. Evaluation of reconstructed images with different voxel sizes of acquisition in the diagnosis of simulated external root resorption using cone beam computed tomography. Int Endod J 2012;45:234-9.
28. Kamburoğlu K, Murat S, Yüksel SP, Cebeci AR, Paksoy CS. Occlusal caries detection by using a cone-beam CT with different voxel resolutions and a digital intraoral sensor. Oral Surg Oral Med Oral Pathol Oral Radiol Endod 2010;109:63-9.
29. Özer SY. Detection of vertical root fractures by using cone beam computed tomography with variable voxel sizes in an in vitro model. J Endod 2011;37:75-9.
30. Torres MG, Campos PS, Segundo NP, Navarro M, Crusoé-Rebello I. Accuracy of linear measurements in cone beam computed tomography with different voxel sizes. Implant Dent 2012;21:150-5.
31. Dawood A, Brown J, Sauret-Jackson V, Purkayastha S. Optimization of cone beam CT exposure for pre-surgical evaluation of the implant site. Dentomaxillofac Radiol 2012;41:70-4.
32. Morant JJ, Salvadó M, Hernández-Girón I, Casanovas R, Ortega R, Calzado A. Dosimetry of a cone beam CT device for oral and maxillofacial radiology using Monte Carlo techniques and ICRP adult reference computational phantoms. Dentomaxillofac Radiol. [In press].
33. Grünheid T, Schieck JRK, Pliska BT, Ahmad M, Larson BE. Dosimetry of a cone-beam computed tomography machine compared with a digital X-ray machine in orthodontic imaging. Am J Orthod Dentofacial Orthop 2012;141:436-43.
34. Ludlow JB, Ivanovic M. Comparative dosimetry of dental CBCT devices and 64-slice CT for oral and maxillofacial radiology. Oral Surg Oral Med Oral Pathol Oral Radiol Endod 2008; 106:106-14.
35. International Commission on Radiological Protection. Recommendations of the International Commission on Radiological Protection. ICRP publication. Ann ICRP 2007:37:1-332.
36. Safety and Efficacy of a New and Emerging Dental X-ray Modality. Radiation protection no. 172: cone beam CT for dental and maxillofacial radiology (evidence-based guidelines). 2012. Available at: http://www.sedentexct.eu/files/radiation_protection_172.pdf.
37. Liang X, Jacobs R, Hassan B, Li L, Pauwels R, Corpas L, et al. A comparative evaluation of cone beam computed tomography (CBCT) and multi-slice CT (MSCT) Part I. On subjective image quality. Eur J Radiol 2010;75:265-9.

Reprint requests:

Sergio Lins de-Azevedo-Vaz
Division of Oral Radiology
Department of Oral Diagnosis
Piracicaba Dental School
State University of Campinas
901, Limeira Avenue, PO Box 52
13414-903, Piracicaba, SP
Brazil
sergiolinsv@gmail.com